ELSEVIER

Journal of Non-Crystalline Solids 209 (1997) 149–158

JOURNAL OF NON-CRYSTALLINE SOLIDS

Structure of Ag–As–Se glasses with high silver content X-ray diffraction and reverse Monte Carlo simulations

N. Zotov *, F. Bellido, R. Jimenez-Garay

Departamento de Fisica de la Materia Condensada, University of Cadiz, 11510 Puerto Real (Cadiz), Spain

Received 31 October 1995; revised 2 April 1996

Abstract

The structure of ternary Ag–As–Se chalcogenide glasses $(Ag_2Se)_x(AsSe)_{1-x}$, where $x = 0.27$, 0.39 and 0.54, have been studied by X-ray diffraction radial distribution function analysis. The average coordination number increases from 2.5 ± 0.1 to 3.5 ± 0.1 with increasing Ag content, accompanied by a decrease of the medium-range order on the 3–8 Å scale. Using the experimentally determined structure factors, the first three-dimensional models of the structure of Ag–As–Se glasses are constructed by the reverse Monte Carlo (RMC) method. The RMC simulations indicate that the Ag–Se coordination number is 2.5 ± 0.2 in the whole compositional range studied. On the contrary, the average coordination number of Se increases from about 2.8 to 4.0 with increasing Ag content. First estimate of the As–As coordination number, $n_{As}^{As} = 0.6$, in Ag–As–Se glasses is made. With increasing silver content the structure changes from a network of molecular-like units ($AsSe_3$ and $AgSe_3$ pyramids and $AgSe_4$ tetrahedra) connected via –Ag–Se–Ag– and –As–Se–As– chain-like elements to overcoordinated three-dimensional cluster-type structure.

1. Introduction

Ternary Ag–As–Se chalcogenide glasses are formed in a large homogeneous glass-formation region centered about the $(Ag_2Se)_x(AsSe)_{1-x}$ tie line [1]. The interest towards these materials was largely stimulated by the fact that their electric conductivity changes from predominantly electronic at low Ag contents to predominantly ionic at high Ag contents [2,3].

The local structure of the Ag–As–Se glasses has been studied by extended X-ray absorption fine structure (EXAFS) spectroscopy [4], the isotopic substitution method in neutron diffraction [5,6] and X-ray diffraction radial distribution functions analysis [7,8]. Based on their EXAFS results, Mastelaro et al. [4] have proposed a schematic picture of the local structure of the Ag–As–Se glasses with $0.11 \leq x \leq 0.43$. However, despite the efforts of earlier workers, the structure of these glasses is still poorly understood and some of the data are even contradictory. The average Ag–Se coordination number for the composition $x = 0.25$, $n_{Ag}^{Se} = 4.0 \pm 0.2$, determined by neutron diffraction [6] is significantly higher than that obtained from the EXAFS measurements [4] ($n_{Ag}^{Se} = 2.0 \pm 0.2$). The EXAFS results, obtained in a large compositional range, indicate that not all silver atoms are four-fold coordinated, as suggested by the formal valence shell (FVS) model, proposed by Liu and Taylor [9].

* Corresponding author. Permanent address: Central Laboratory of Mineralogy and Crystallography, Rakovski Street 92, Sofia 1000, Bulgaria. E-mail: nzotov@czvl.uca.es.

PII S0022-3093(96)00538-8

The X-ray diffraction studies of Ag–As–Se glasses with low silver content [7,8] are consistent with the hypothesis for 4-coordinated silver and has revealed the presence of a strong first sharp diffraction peak (FSDP), considered as manifestation of the medium-range order (MRO) in covalently bonded glasses [10,11]. Therefore, structural investigations of $(Ag_2Se)_x(AsSe)_{1-x}$ glasses with high silver content ($x > 0.25$) and the generation of realistic three-dimensional models of their structure, which would allow detailed analysis of the changes both in the short-range order (SRO) and the MRO with composition, are necessary.

In the past there were numerous analyses of single wavelength X-ray diffraction radial distribution functions (RDF) of binary As–Se and ternary Ag–Ge(As)–Se glasses, using either the microcrystalline approach [12] or empirical expressions relating the area under the first RDF peak with the concentration and the possible coordination of the constituent atoms [13,14].

The relatively novel reverse Monte Carlo (RMC) method [15] gives an alternative approach for modeling and interpretation of the structure of disordered materials and has been successfully applied to many different glasses and liquids [16]. The RMC method generates atomic configurations, consistent with the whole diffraction data set(s), and not just fitting particular features like the area under the first RDF peak. Of course, if we have only one set of data and the atom scattering factors are similar, as in the case of As and Se, then it is unlikely that all the 6 partial pair distribution functions of a 3 component Ag–As–Se glass will be very reliable but they certainly will be no worse than any other qualitative analysis of the data that can be done. However, the RMC method allows additional structural information to be taken into account in the form of coordination constraints in order to reduce the possible range of structural models. Besides that the RMC models can be used for analysis of the bond-angle distributions and the distortions of the coordination polyhedra both of which cannot be determined directly from the RDFs but are very important for understanding the electronic and the vibrational properties of the investigated materials.

Correspondingly, the aims of the present paper are: (1) to obtain X-ray diffraction radial distribution functions for several $(Ag_2Se)_x(AsSe)_{1-x}$ glasses with large Ag content ($x \geq 0.25$) and thus to follow the overall changes in the structure with approaching the amorphous-crystalline boundary at about $x = 0.6$ [1]; (2) to construct models of the structure of these glasses consistent with the experimental X-ray diffraction and previous EXAFS [4] data using the reverse Monte Carlo method. Since there are only a few RMC models of Ag-containing ternary chalcogenide glasses [17], the RMC method will not only allow some quantitative interpretation of the structure of the Ag–As–Se glasses to be made but will be a further test of the applicability of the method to ternary chalcogenide glasses in general.

The paper is organized in the following way: Section 2.1 describes the preparation of the samples, details of the X-ray diffraction experiments as well as the radial distribution analysis are given in Section 2.2 and Section 2.3 describes the RMC technique employed. The X-ray diffraction and RMC results are presented in Section 3 and the changes in the structure of the investigated Ag–As–Se glasses with increasing Ag content are discussed in Section 4.

2. Experimental

2.1. Sample preparation and characterization

Three samples along the $(Ag_2Se)_x(AsSe)_{1-x}$ tie line were prepared for the present study. First, pure silver (99.99% Aldrich), arsenic (99.9999% Aldrich) and selenium (99.999% Aldrich) were ground in agate mortar, sieved through a mesh to obtain grain size of less than 64 μm and mixed together to obtain about 8 g of the corresponding composition. For each sample the powder mixture was put into quartz tube of 6 mm inner diameter and repeatedly evacuated – refilled with He. The tube was then sealed with an oxyacetylene burner while the residual gas pressure was about 1×10^{-3} Torr. The as-prepared ampoule was kept at 800°C for 4 days in a furnace and then quenched in ice water. In order to obtain good homogeneity of the samples, the ampoules were rotating with about 6 rmp. The composition of the final glassy alloys was determined using a Jeol JSM 820 SEM with EDAX X-ray dispersive analyser. The mass density of the samples was measured

Table 1
Composition, bulk density (ρ), number density (ρ_0), glass transition temperatures (T_g) and mean standard deviations $\langle\sigma_g\rangle$ for the investigated Ag–As–Se chalcogenide glasses

Sample	ρ (g/cm^3)	ρ_0 (atoms/Å^3)	Composition			T_g (K)	$\langle\sigma_g\rangle$
			Ag	As	Se		
AG27	5.40(2) [a]	0.0385(1) [b]	0.236(1) [c]	0.324(9) [c]	0.440(9) [c]	430(1) [a]	0.06
AG39	5.53(4)	0.0381(3)	0.328(7)	0.256(1)	0.416(7)	433(1)	0.07
AG54	6.20(5)	0.0411(20)	0.419(7)	0.179(6)	0.402(6)	430(2)	0.03

[a] The standard deviations, given in parentheses, are determined from 3 measurements.
[b] The standard deviations, given in parentheses, are calculated as $\sigma(\rho_0) = (A/M)\sigma(\rho)$, where $\sigma(\rho)$ is the standard deviation in the bulk density, A is the Avogadro number and M is the molecular weight.
[c] The standard deviations, given in parentheses, are determined from at least 7 measurements.

picnometrically. The glass transition temperatures (T_g) were measured by Perkin-Elmer DSC 7 thermal analyser.

The composition, the densities and T_g for the investigated samples are listed in Table 1. The x values of the samples along the $(Ag_2Se)_x(AsSe)_{1-x}$ tie line are 0.27, 0.39 and 0.54. That is why the samples will be denoted hereafter as AG27, AG39 and AG54, respectively. The mass density and T_g for the AG27 sample compares well with the data for $Ag_{22.2}As_{33.3}Se_{44.4}$ ($x = 0.25$) measured by Benmore and Salmon [5].

2.2. X-ray diffraction experiments and calculation of the radial distribution functions

The X-ray diffraction experiments were carried out on a Siemens D500 automatic powder diffractometer using Mo K_α radiation (wavelength $\lambda = 0.7109$ Å) equipped with a diffracted beam monochromator ($\Theta_M = 6.095°$, where 2Θ is the diffraction angle) and scintillation detector. All measurements were made in reflection geometry, in the angular range from 5 to 110° 2Θ, corresponding to a Q range from 0.77 Å^{-1} to 14.5 Å^{-1}, where $Q = 4\pi\sin(\Theta)/\lambda$. The spectrum was scanned with a constant step width $\Delta 2\Theta = 0.2°$ from 5° to 70° and with $\Delta 2\Theta = 0.5°$ from 70° to 110°. For each sample the intensities were measured 4 times using 4000 counts per step and the results were averaged. The mean standard deviations $\langle\sigma_I\rangle$ are 0.06, 0.07 and 0.19 counts/s for the AG27, AG39 and AG54 samples, respectively. The averaged data was further Fourier smoothed before the RDF analysis. The background scattering with the sample absent was measured from 5° to 110° 2Θ with step width $\Delta 2\Theta = 0.5°$ using 120 s per step. The background data below 70° 2Θ were interpolated with step width $\Delta 2\Theta = 0.2°$ using cubic spline functions.

The smoothed data for each composition were corrected for background scattering, polarization and absorption in the sample in the usual way [18]. The corrected intensity was converted into electronic units by the Krogh–Moe method [19] and the incoherent scattering was subtracted to obtain the total coherent scattering $I_{coh}(Q)$. The incoherent scattering was calculated from published regression coefficients [20], taking into account the Breit–Dirac recoil factor and the bandpass of the monochromator which was determined using the method of Ruland [21].

The reduced structure factor, $F(Q)$, which represents a weighted sum of all partial structure factors $A_{ij}(Q)$, $F(Q) = \sum_{ij}\gamma_{ij}(Q)(A_{ij}(Q) - 1)$, was calculated from the total coherent scattering by $F(Q) = (I_{coh}(Q) - \langle f^2\rangle)/\langle f\rangle^2$, where $\langle f\rangle^2 = \sum_{ij}c_ic_jf_if_j^*$, $\langle f^2\rangle = \sum_i c_i f_i f_i^*$, f_i is the atomic form factor for atom species i and the summation is over all atoms in the structural unit. The Q-dependent coefficients $\gamma_{ij}(Q)$ are defined by $\gamma_{ij}(Q) = c_ic_jf_if_j^*/\langle f\rangle^2$. The atomic scattering factors were calculated from analytical expressions [22] and corrected for anomalous dispersion [23].

The reduced radial distribution function $G(r)$ was then calculated as the Fourier transform of the reduced structure factor:

$$G(r) = 2/\pi\int QF(Q)\sin(Qr)M(Q)\,dQ, \qquad (1)$$

where the modification function $M(Q)$ was chosen in the form proposed by Lorch [24], $M(Q) = \sin(\alpha Q)/(\alpha Q)$. The α values were determined from the condition $M(Q_{max}) = 0.01$. The total pair correlation function is calculated then by $T(r) = 4\pi\rho_0 r + G(r)$, where ρ_0 is the atom number density of the glass. The total pair distribution function (TPDF), $g(r)$, which is used in the RMC simulations, is related to $T(r)$ by $g(r) = T(r)/4\pi\rho_0 r$. The corresponding $T(r)$ and $F(Q)$ functions were corrected for small residual errors using the method of Kaplow et al. [25].

The RMC method requires some initial estimate of the experimental errors to be provided for each data set. That is why an analysis of the statistical errors in the structure factors, $F(Q)$, and the corresponding $g(r)$ functions was carried out. The standard deviation of the total structure factor, $\sigma_F(Q)$, can be related to the standard deviation of the raw data $\sigma_I(Q)$ by

$$\sigma_F(Q) = \frac{\beta A(Q) P(Q)}{\langle f \rangle^2} \sqrt{\sigma_I^2(Q) + \sigma_B^2(Q)}\,, \quad (2)$$

where β is the normalization constant, $A(Q)$ is the absorption correction, $P(Q)$ is the polarization correction and $\sigma_B(Q)$ is the standard deviation of the background.

The standard deviation of $T(r)$, $\sigma_T(r)$, is calculated then, assuming independence of the $\sigma_F(Q)$ errors at the different Q points, by:

$$\sigma_T^2(r) = \left(\frac{2}{\pi}\Delta Q\right)^2 \sum_Q Q^2 M^2(Q) \sin^2(Qr) \sigma_F^2(Q) + (4\pi r)^2 \sigma_\rho^2, \quad (3)$$

where ΔQ is the step used for calculating the $F(Q)$ function and σ_ρ^2 is the standard deviation of the atom number density. Finally the standard deviation in the TPDF is calculated by $\sigma_g(r) = \sigma_T(r)/4\pi r\rho_0$. Since a uniform error distribution σ is normally used in the RMC algorithm, the $\sigma_F(Q)$ and $\sigma_g(r)$ distributions were averaged. The corresponding mean $\langle \sigma_g \rangle$ values are listed in Table 1. All calculations were performed using the program RADIF [26].

2.3. RMC simulations

Although it has been demonstrated that the area of the first X-ray diffraction RDF peak is insensitive to the actual number of As–Se, As–As and Se–Se bonds [27–30], there is large amount of experimental evidence (from compositionally related crystalline phases [31–34], vibrational spectroscopy [35] and EXAFS [4]) for the presence of chemical short-range ordering (CSRO) in the Ag–As–Se glasses. That is why in the present paper only RMC models with chemical short-range ordering are considered.

In order to model the CSRO, the following fractional coordination constraints excluding the formation of short homopolar bonds (bond lengths < 2.9–3.0 Å) were applied: (i) the possibility of short Ag–Ag bonds was excluded on the basis of the neutron diffraction results for $x = 0.25$ [6], the low temperature Ag K_α EXAFS data [4] for $x = 0.43$ and the absence of short Ag–Ag distances in the crystalline Ag_2Se [33] and Ag_3AsSe_3 [34] crystalline compounds; (ii) the formation of short Se–Se bonds was forbidden on the basis of comparison with the Se–Se bond lengths in crystalline As_4Se_4 [31], As_2Se_3 [32], Ag_2Se [33] and Ag_3AsSe_3 [34] compounds; (iii) the possibility for short Ag–As bonds was also excluded on chemical grounds since Ag and As are practically immiscible at room temperature [36]. Several additional coordination constraints, based on the EXAFS [4] and neutron [6] results, were applied: $n_{Ag}^{Se} \leq 5$, $n_{As}^{Se} \leq 3$, $n_{As}^{As} \leq 1$, $n_{Se}^{Ag} > 1$ and $n_{Se}^{As} > 1$, which prevent the formation of under- or over-coordinated atoms.

Starting configurations of 1000 particles with appropriate composition (see Table 1), *randomly* distributed in a cubic box of edge length $L \approx 30$ Å with periodic boundary conditions, were used in all three cases. The RMC requirement, $g(r) \equiv 1$ for $r > L/2$, was strictly fulfilled for all compositions because there are no structural oscillations in the corresponding TPDF functions for $r > 10$ Å (see below). The starting configurations were generated with a distance of closest approach between any two particles equal 1.9 Å, which corresponds to the low r limit of the first peak in the corresponding TPD functions.

The RMC simulations were performed using a two-stage procedure: (1) RMC fits were made first to the corresponding $g(r)$ function with coefficients of

the partials equal to $\gamma_{ij}(Q=0)$ and $\sigma=0.05$, a reasonable value in regard of the mean $\langle \sigma_g \rangle$ errors listed in Table 1; (2) after a structural equilibrium was achieved and all coordination constraints were fulfilled, a final fit to the corresponding TSF was made with the actual Q-dependent coefficients $\gamma_{ij}(Q)$, reducing σ gradually to 0.01. Such an approach is not only much less time consuming but is justified by the fact that the corresponding $\gamma_{ij}(Q)$ coefficients are in first approximation independent of Q. The term 'structural equilibrium' will be used hereafter to denote the case when the goodness-of-fit factor, χ^2, starts to oscillate around a given value without significant improvement of the fit between the experimental and calculated TSF or TPDF.

All calculations were performed on a VAX 4100 computer using the RMCA program [37]. Structural equilibrium in the final $F(Q)$ fits was achieved after about 30 h. The final χ^2 goodness-of-fit factors are close to 1.0.

3. Results

Fig. 1 shows the simulated reduced structure factors, $F(Q)$, compared with the experimental data for

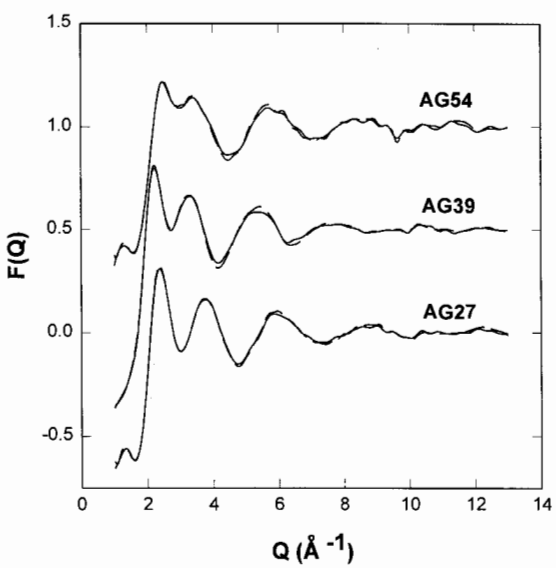

Fig. 1. Final RMC fits to the total structure factors for the AG27, AG39 and AG54 samples: (————) experimental diffraction data, (---) RMC data. The data for the AG39 and AG54 samples are shifted by 0.5 and 1.0 units for clarity.

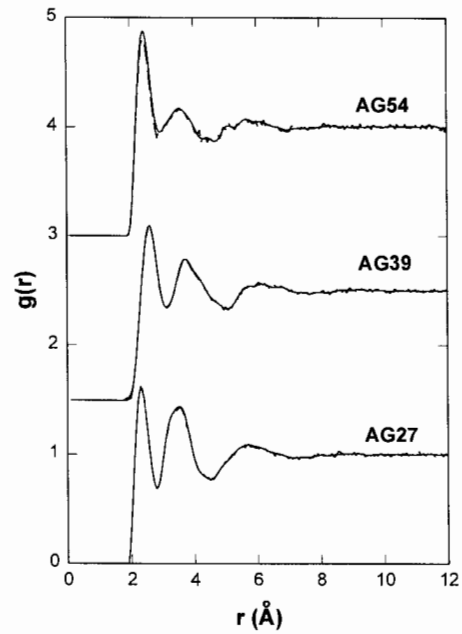

Fig. 2. Experimental and calculated total pair distribution functions for the AG27, AG39 and AG54 samples: (————) experimental X-ray diffraction data, (---) RMC data. The data for the AG39 and AG54 samples are shifted by 1.5 and 3.0 units for clarity.

the three compositions. The experimental and the simulated total pair distribution functions, $g(r)$, are given in Fig. 2. The RMC fits reproduce very well all the features of the corresponding $g(r)$ and $F(Q)$ functions, in particular the first sharp diffraction peak (FSDP) observed at about 1.2 Å^{-1} in samples AG27 and AG54.

Comparison of the intensity of the FSDP in the investigated Ag–As–Se glasses with high Ag content and in Ag–As–Se glasses with low Ag content [7,8] (although not exactly on the Ag_2Se–AsSe tie line) indicates that the MRO in the Ag–As–Se glasses changes significantly with increasing the Ag content. The absence of FSDP in the AG39 sample indicates, however, that the MRO in these glasses is possibly also very sensitive to small changes in the silver content.

All samples exhibit three $g(r)$ peaks at about 2.6, 3.7 and 5.5 Å. There are no structural oscillations beyond 10 Å for all compositions. However, significant changes below 10 Å are observed with increasing Ag content. The average coordination number,

determined as the area under the first peak in the corresponding total radial distribution function, $rT(r)$, increases non-linearly with increasing Ag content (see Table 2). At the same time the second and the third $g(r)$ peaks decrease in intensity, suggesting a decrease of the MRO on the 3–8 Å scale.

The comparison of the partial pair distribution functions (PPDF), determined from the RMC models, indicates that most significant changes are in the Ag–Ag, Ag–Se and the As–Se PPDF, shown in Fig. 3a–c, using a reduced scale r/r_M, where r_M is the position of the first maximum in the corresponding PPDF. The Ag–Ag first-nearest neighbor (Ag–Ag1) distribution broadens significantly with increasing Ag content. As a consequence, the Ag–Ag1 coordination number increases strongly in the range $0.3 < x$

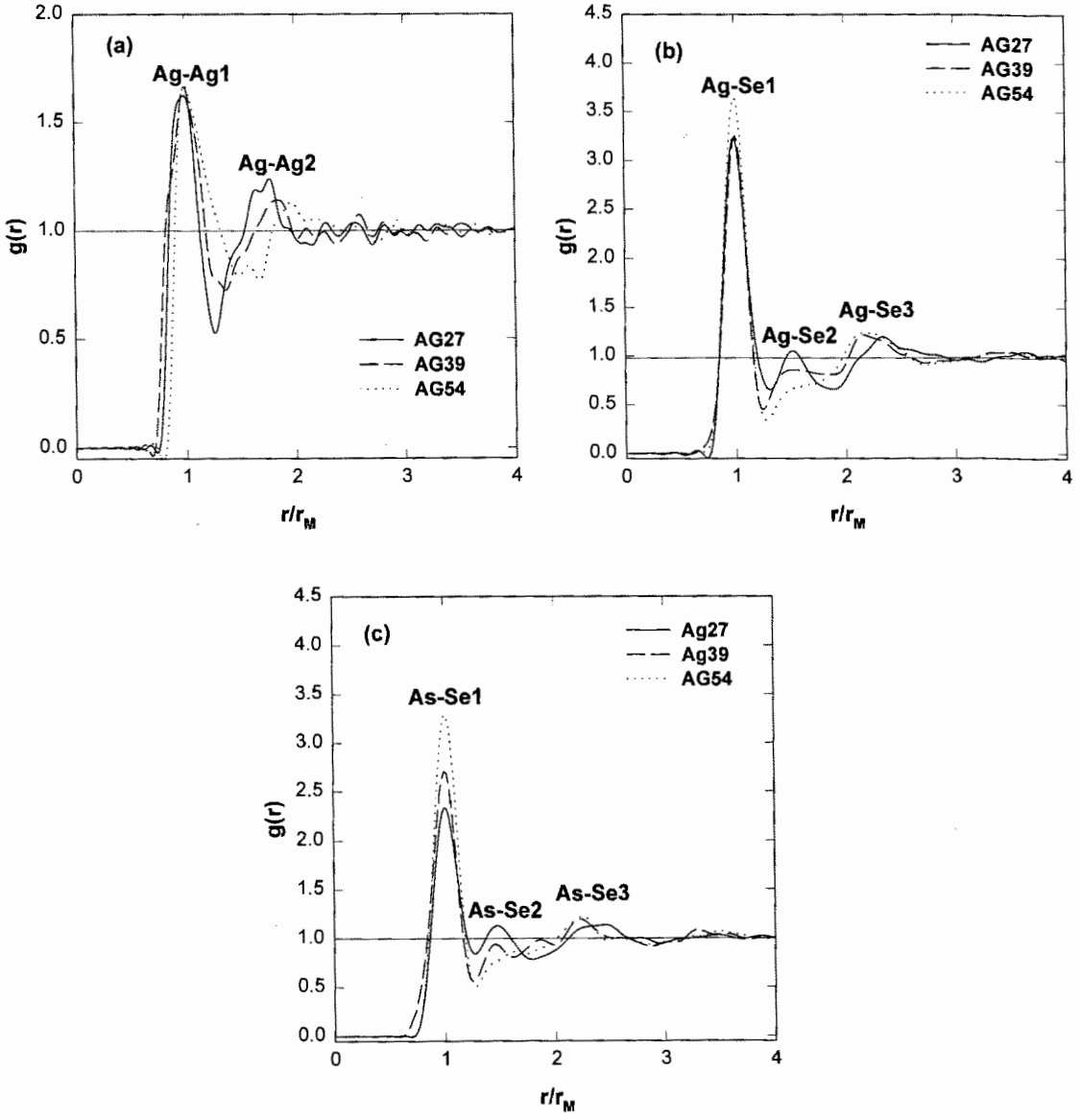

Fig. 3. Partial pair distribution functions (PPDF), calculated from the RMC fits: (a) Ag–Ag PPDF; (b) Ag–Se PPDF; (c) As–Se PPDF.

Table 2
Average coordination numbers of the investigated Ag–As–Se glasses

Atom	Composition								
	AG27			AG39			AG54		
	RDF	RMC	EXAFS [a]	RDF	RMC	EXAFS [a]	RDF	RMC	EXAFS [a]
Ag	—	2.4 ± 1.1	2.0	—	2.7 ± 1.1	2.0	—	2.7 ± 1.0	2.0 [c]
As	—	2.5 ± 0.8	3.0	—	3.1 ± 0.8	3.0	—	3.2 ± 0.8	3.0 [c]
Se	—	2.8 ± 0.8	2.4 [b]	—	3.7 ± 0.9	2.85 [b]	—	4.0 ± 0.9	3.7 [c]
Average	2.5 ± 0.1	2.6	2.5 [d]	3.5 ± 0.1	3.2	2.6 [d]	3.3 ± 0.1	3.3	2.9 [d]

[a] Ref. [4].
[b] Interpolated values.
[c] Extrapolated values.
[d] Calculated from the EXAFS [4] coordination numbers for the corresponding atoms and the composition of the samples determined in the present study.

< 0.4 from 2.8 ± 1.5 for the AG27 sample to about 6.5 ± 1.5 in AG39 and AG54. The Ag–Ag1 coordination number for the AG27 sample, 2.8 ± 1.5, compares very well with the value, 2.7 ± 0.2, determined by the isotopic substitution method in neutron diffraction [6] for the Ag–As–Se glass with $x = 0.25$.

The comparison of the partial structure factors indicates that the most significant changes are in the Ag–Se partial structure factors (Fig. 4). The shift of the second and the third Ag–Se peaks to lower Q values accounts well for the observed changes in the corresponding total structure factors. It is interesting to note that the Ag–Se partial structure factor for $x = 0.54$ is very similar to that in molten Ag_2Se, calculated by molecular dynamics [38].

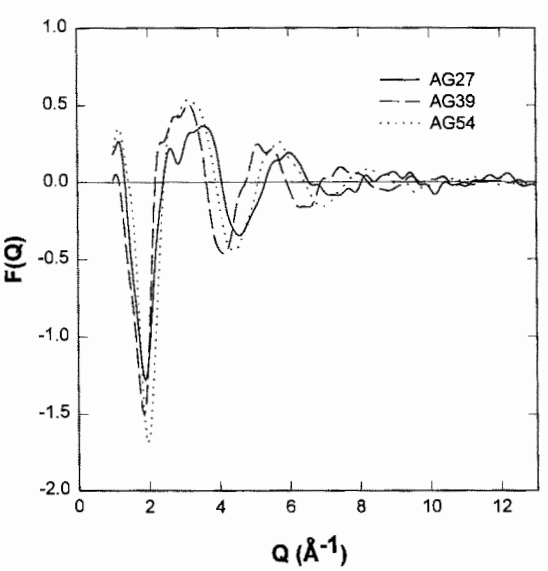

Fig. 4. Partial Ag–Se structure factors, calculated from the RMC models: AG27 (————), AG39 (---) and AG54 (· · ·) samples.

4. Discussion

4.1. Short-range order

The variation of the average coordination numbers, calculated from the RMC models, compares well with the experimentally observed increase of the average coordination number with increasing Ag content (see Table 2). The average coordination number for the AG27 sample, calculated from the EXAFS data [4], is also in very good agreement with the RDF results, but the coordination numbers calculated for the AG39 and AG54 samples are lower. This fact indicates that some of the corresponding EXAFS coordination numbers are possibly underestimated.

The Ag–Se average coordination number practically remains constant, $n_{Ag}^{Se} = 2.5 \pm 0.2$, with increasing silver content. The RMC results give thus further evidence that the Ag coordination does not change with composition, as indicated by previous neutron diffraction [5] and EXAFS [4] measurements.

The geometrical analysis of the models indicates that the Ag atoms form a network of distorted $AgSe_3$ pyramidal units and $AgSe_4$ tetrahedra with additional

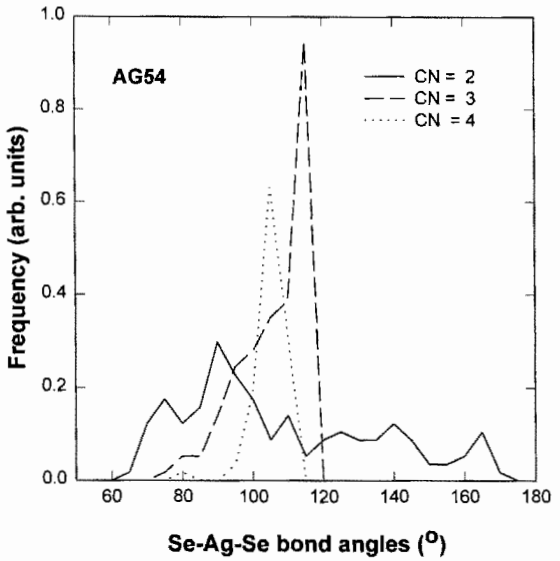

Fig. 5. Se–Ag–Se bond angle distributions for the 2 (————), 3 (---) and 4 (· · ·) coordinated Ag atoms in the RMC model of the AG54 sample.

–Ag–Se–Ag– chain-like elements. A slight increase of the three-coordinated atoms is encountered with increasing Ag content at the expense of a corresponding decrease of the Ag atoms bonded to one or two Se atoms. The fraction of the 4-coordinated Ag atoms is about $17 \pm 5\%$. The Se–Ag–Se bond angle distributions for the 2-, 3- and 4-coordinated Ag atoms are quite different (see Fig. 5). The Se–Ag–Se bond angles (α) for the 2-coordinated Ag atoms have almost *random* distribution in the range 60–180° with a weak and broad maximum peaked at about 90°, the FWHM of which increases with increasing Ag content. On the contrary, the average α values for the 4-coordinated silver atoms have a narrow distribution (FWHM ~ 5°), peaked close to the ideal tetrahedral value. Most interesting is the distribution of the Se–Ag–Se bond angles for the 3-coordinated Ag atoms. In all three samples it is zero for $\alpha > 120°$, has a maximum for α slightly less than 120° and smoothly decreases to zero at about 60–65°. Such behaviour can be roughly understood assuming that all $AgSe_3$ units represent regular triangular pyramids with axial distortion h/R, where h is the height of the pyramid and R is the length of the Ag–Se bonds. In this case the cosine of the Se–Ag–Se angle (α) can be written in the form, $\cos(\alpha) = -0.5 + 3(h/R)^2$. Therefore the Se–Ag–Se distributions indicate that the axial distortions of the $AgSe_3$ pyramids varies continuously with most of the Ag atoms in planar triangular coordination ($h/R = 0.0$). The relative amount of triangularly coordinated Ag atoms increases with increasing Ag content. The different types of Ag coordination established in the RMC models are in full agreement with the data for the Ag_2Se [33] and Ag_3AsSe_3 [34] compounds. In Ag_2Se [33] one half of the silver atoms are almost tetrahedrally coordinated and the other half are triangularly coordinated, while in Ag_3AsSe_3 [34] the Ag atoms form –Ag–Se–Ag– chains connecting the $AsSe_3$ pyramids.

The average coordination of arsenic is close to 3.0 in all three samples (see Table 2) in agreement with the EXAFS [4] results. The As–As first-nearest neighbor (As–As1) coordination number also does not change with composition. The value obtained from the RMC simulations, $n_{As}^{As} = 0.6 \pm 0.8$, is of special interest, since it is well known that EXAFS spectroscopy cannot resolve the Se and As contributions. The As atoms form a network of distorted $AsSe_3$ pyramids and –As–Se–As– chain-like elements with some $As(AsSe_3)$ tetrahedral or square pyramidal units in addition. The Se–As–Se bond angles for the 2-coordinated As atoms have a broad distribution in the range 60–180° which becomes more random with increasing Ag content. The average Se–As–Se bond angles of the $AsSe_3$ pyramids vary continuously from 120° (planar coordination) to about 65° (while all Se–As–Se bond angles in the Ag_3AsSe_3 [34] phase are equal to 98°).

Most significant is the change of the Se average coordination number. It increases from 2.8 to 4.0 with increasing Ag concentration. The X-ray RDF studies of Ag–Ge–Se glasses [14] also indicate that the chalcogen coordination number increases from 2.7 to 4.0 with increasing Ag concentration. The increase of the average Se coordination results from two counterpart mechanisms – a slight decrease of the Se–As first nearest neighbor coordination number and increase of the Se–Ag first nearest neighbor (Se–Ag1) coordination number. The Se–Ag1 coordination numbers obtained 1.3 ± 0.5, 2.2 ± 0.9 and 2.7 ± 0.9 for the Ag27, AG39 and AG54 samples, respectively, follow closely the EXAFS results [4].

4.2. Medium-range order

The increase of the number of the Se–Ag bonds leads to significant changes in the glassy network: the proportion of the molecular-like elements decreases while the branching of the –Ag–Se–Ag–(–As–Se–As–) chains and the connectivity of the network as a whole increases (see Fig. 6).

In addition, the intensity of the Ag–Se second-nearest neighbor (Ag–Se2) and the As–Se second-nearest neighbor (As–Se2) peaks in the range 3–5 Å systematically decreases with increasing Ag content (see Fig. 3b and Fig. 3c), while the magnitude of the Ag–Ag1 correlations (see Fig. 3a), as well as the Se–Se1 and the As–As2 correlations (not shown in Fig. 3), remain practically unchanged. Taking into account the variation of the $\gamma_{ij}(Q)$ coefficients with composition, it may be concluded that the observed decrease of the intensity of the second peak in the TPDF with increasing Ag content (see Fig. 2) results from: (i) the decrease of the γ_{AsAs} and γ_{SeSe} coefficients and (ii) the decrease in As–Se second-nearest neighbor correlations (the decrease in the Ag–Se2 correlations is almost compensated by the increase of the γ_{AgSe} coefficient).

Preliminary analysis of the density fluctuations in the three models indicates that the AG39 structure is most homogeneous. This might be connected with the fact that the FSDP disappears in this alloy and will be a subject of future studies.

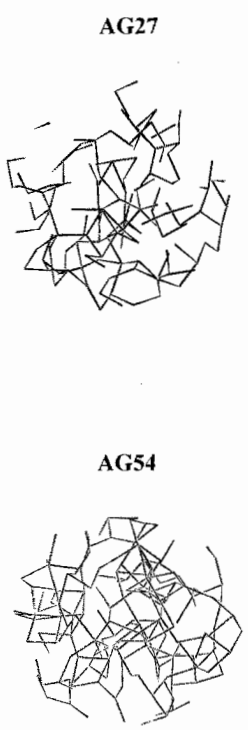

Fig. 6. Networks of Ag–Se and As–Se bonds in spherical sections (radius 10 Å) of the RMC models for the AG27 and AG54 samples.

5. Conclusions

X-ray diffraction investigation of three Ag-containing chalcogenide glasses $(Ag_2Se)_x(AsSe)_{1-x}$, with high silver content ($x = 0.27$, 0.39 and 0.54) was carried out. Models of the structure were generated using reverse Monte Carlo (RMC) fits to the total X-ray diffraction structure factors with chemical short-range ordering coordination constraints. The main results can be summarised as follows:

(1) An abrupt increase of the average coordination number is observed for $x > 0.3$. The RMC simulations indicate that it is mainly due to the increase of the Se coordination from 2.8 to about 4.0.

(2) The Ag–Se coordination number, on the contrary, remains practically unchanged. The Ag atoms are bonded on average to 2.5 ± 0.2 Se atoms. Significant number of Ag atoms have planar triangular coordination similar to that in the crystalline phase Ag_2Se [33]. The Ag–Ag first-nearest neighbor coordination increases with increasing Ag content, which might indicate some clustering of the Ag atoms at high Ag contents.

(3) The average As coordination is close to 3.0 with the As atoms coordinated on average by 0.6 ± 0.8 As atoms in all three samples. The additional As–As bonds lead to the formation of distorted $As(AsSe_3)$ tetrahedral or square pyramidal units.

(4) A decrease of the intensity of the second peak in the total pair distribution functions with increasing Ag content is observed. It is due both to a change in the weighted scattering coefficients $\gamma_{ij}(Q)$ and to a decrease of the As–Se as well as the Ag–Se second-nearest neighbor correlations.

(5) The structure of the investigated Ag–As–Se glasses can be described as network of molecular-like $AsSe_3(AgSe_3)$ pyramidal units and $AgSe_4$ tetrahe-

dra, connected by –As–Se–As– (–Ag–Se–Ag–) chain-like elements.

(6) Finally, we demonstrated that RMC fits to single-wavelength X-ray diffraction data from ternary chalcogenide glasses can produce reasonable structural models if proper chemical short-range order coordination constraints are imposed.

Acknowledgements

The authors would like to thank J. González for the help in performing the electron probe analyses as well as R. McGreevy and the referee for the constructive suggestions concerning the revised version of the paper. N.Z. acknowledges the financial support from the Spanish Interministerial Commission of Science and Technology.

References

[1] D. Houphouet-Boigny, R. Ollitrault-Fichet, R. Eholie and J. Flahaut, Mater. Res. Bull. 22 (1987) 169.
[2] Z.U. Borisova, Glassy Semiconductors (Plenum Press, New York, 1981).
[3] C. Carcaly and D. Houphouet-Boigny, J. Non-Cryst. Solids 86 (1986) 271.
[4] V. Mastelaro, S. Banazeth, H. Dexpert, A. Ibanez and R. Ollitrault-Fichet, J. Non-Cryst. Solids 151 (1992) 1.
[5] C.J. Benmore and P.S. Salmon, J. Non-Cryst. Solids 156–158 (1993) 720.
[6] C.J. Benmore and P.S. Salmon, Phys. Rev. Lett. 73 (1994) 264.
[7] F. Bellido, P. Villares and R. Jimenez-Garay, in: The Physics of Non-Crystalline Solids, eds. L.D. Pye, W.C. LaCrouse and H.J. Stevens (Taylor and Francis, London, 1992) p. 77.
[8] F. Bellido, J. Vazquez, P. Villares and R. Jimenez-Garay, Phys. Scr. 50 (1994) 566.
[9] J.Z. Liu and P.C. Taylor, J. Non-Cryst. Solids 114 (1989) 25.
[10] S.R. Elliot, Phys. Rev. Lett. 67 (1991) 711.
[11] A.P. Sokolov, A. Kisliuk, M. Solotwish and D. Quitmann, Phys. Rev. Lett. 69 (1992) 1540.
[12] A.L. Reninger and B.L. Averbach, Phys. Rev. B8 (1973) 1507.
[13] J. Vazquez, M. Casas-Ruiz, R.A. Ligero and R. Jimenez-Garay, Mater. Chem. Phys. 32 (1992) 63, and references therein.
[14] L.C. Bourne, S.C. Rowland and A. Bienenstock, J. Phys. C4 (1981) 951.
[15] R. McGreevy and L. Pusztai, Mol. Simulations 1 (1988) 359.
[16] R.L. McGreevy and M.A. Hove, Ann. Rev. Mater. Sci. 22 (1992) 217.
[17] J.H. Lee, A.P. Owens and S.R. Eliot, J. Non-Cryst. Solids 164–166 (1993) 139.
[18] A.C. Wright, Adv. Struct. Dev. Diffr. Meth. 5 (1974) 1.
[19] J. Krogh-Moe, Acta Crystallogr. 9 (1956) 951.
[20] H.H.M. Balyuzi, Acta Crystallogr. A31 (1975) 600.
[21] W. Ruland, Br. J. Appl. Phys. 15 (1964) 1301.
[22] D.T. Cromer and J.B. Man, Acta Crystallogr. A24 (1968) 321.
[23] D.T. Cromer, Acta Crystallogr. 18 (1968) 17.
[24] E. Lorch, J. Phys. C2 (1969) 229.
[25] R. Kaplow, B.L. Averbach and S.L. Strong, J. Phys. Chem. Solids 25 (1964) 1196.
[26] N. Zotov, Proc. of 2nd Natl. Conf. X-ray Diffraction Meth. 20–22 May 1985, Primorsko, Bulgaria (Sofia Univ. Press, 1985) pp. 134–139.
[27] J. Chang and D.B. Dove, J. Non-Cryst. Solids 16 (1974) 72.
[28] A.J. Leadbetter and A.J. Apling, J. Non-Cryst. Solids 15 (1974) 250.
[29] K.S. Liang, J. Non-Cryst. Solids 18 (1975) 197.
[30] A.L. Renninger, M.D. Rechtin and B.L. Averbach, J. Non-Cryst. Solids 16 (1974) 1.
[31] P. Goldstain and A. Paton, Acta Crystallogr. B30 (1974) 915.
[32] A.C. Stergiou and P.J. Rentzeperis, Z. Kristallogr. 173 (1985) 185.
[33] G.A. Wiegers, Am. Mineral. 56 (1971) 1882.
[34] K. Sakai, T. Koide and T. Matsumoto, Acta Crystallogr. B34 (1978) 3326.
[35] G. Lukovski and R.M. Martin, J. Non-Cryst. Solids 8–10 (1972) 185.
[36] T.B. Massalski, Binary Alloy Phase Diagrams, 2nd Ed. (ASM Int., Materials Park, OH, 1990).
[37] R. McGreevy, M.A. Hove and J.D. Wicks, RMCA – A General Purpose Reverse Monte Carlo Code, Version 3, October 1993.
[38] J.P. Pino, Y.M.M. Hornas, G.A. Antono, I. Ebbsjo, R.K. Kalia and P. Vashishta, J. Chem. Phys. 89 (1988) 7542.